Magnetospheric convection and thermal ions in the dayside outer magnetosphere

S.-H. Chen[1] and T. E. Moore[2]

Received 16 February 2005; revised 2 December 2005; accepted 4 January 2006; published 18 March 2006.

[1] We have surveyed 3.5 years of Polar Thermal Ion Dynamics Experiment (TIDE) data between 1 January 2000 and 30 June 2003, when Polar apogee paths (sections of orbits with geocentric distances $r > 5\ R_E$) were in the dayside outer magnetosphere, to study the spatial distribution of thermal ions and the magnetospheric convection paths of the thermal ions, as a function of interplanetary magnetic field (IMF) orientation. We have found a dawn-dusk asymmetry in the occurrence of detectable thermal ions above the instrument threshold. The occurrence rate was significantly higher at the duskside. The probability of observing thermal ions, particularly at 1300–1600 local time (LT) near the magnetopause, was >50%, compared with <30% at the dawnside. We interpret the thermal ion events as the result of plasmaspheric drainage plumes, as observed by IMAGE spacecraft or geosynchronous orbiters. The episodic appearance of the thermal ions in the outer magnetosphere could be a significant factor for the dynamo process of global magnetospheric convection. The variation of the convection pattern due to the IMF orientation is consistent with equatorward and poleward reconnection scenarios that superimpose dayside convection driven by reconnection on top of the background convection driven by a viscous interaction at the magnetopause, together with the corotation of the magnetospheric plasma with the ionosphere.

Citation: Chen, S.-H., and T. E. Moore (2006), Magnetospheric convection and thermal ions in the dayside outer magnetosphere, *J. Geophys. Res.*, *111*, A03215, doi:10.1029/2005JA011084.

1. Introduction

[2] Sequences of snapshots of the plasmasphere and surrounding media by the remote sensing instruments on IMAGE spacecraft [*Sandel et al.*, 2001, 2003; *Goldstein et al.*, 2003a] have visualized the evolution of plasma plumes that grow out of the plasmasphere and extend beyond geosynchronous orbit toward the dayside. The evolutionary timescale is less than 4 hours, much shorter than the previously believed timescale of a day or more. Pioneering work by *Chen and Wolf* [1972] and *Chen and Grebowsky* [1974] showed that the evolution of plasma plumes is a function of the geomagnetic activity characterized by the *Kp* index. They compared their model results with observations from the OGO 5 spacecraft [*Chappell*, 1972] and concluded that the plasma plumes exhibit a 6-day timescale as global-scale phenomena. As plasma plumes grow out from the main body of the plasmasphere, they reach the dayside magnetopause boundary within a few hours depending upon the strength of convective electric field and local time where the plasma plumes originate [*Grebowsky*, 1970]. Because of the 3-hour time resolution of *Kp*, it is limited as a measure of convection strength, though it was perhaps the best measure of geomagnetic activity at that time The short timescales of the cold thermal ion plasma plume evolution, as driven by magnetospheric convection, suggests that use of the *Kp* index alone is insufficient. The IMAGE results show that limitations of the coarse *Kp* index, combined with the orbital motion of OGO 5, make it difficult to accurately resolve the true nature of these events without global imaging.

[3] In situ observations from OGO 5 [*Chappell*, 1972] already revealed a dynamic and scattered distribution of cold thermal ions in the outer magnetosphere. As a result, the plasma plumes were described as detached plasma regions. Since the cold thermal ions do not contribute much to the total thermal energy of all ion populations in the outer magnetosphere, the cold thermal ions are not considered as an important component to plasma processes in the region. Recent observations from the Polar spacecraft [*Chen and Moore*, 2004] reinstated *Chappell*'s [1972] finding and further hinted a possible link to magnetic reconnection at the subsolar magnetopause. As a result of data derived from solar wind monitors, magnetospheric orbiters, and ground geomagnetic indices, many recent studies have also found that the plasma plumes were correlated with high geomagnetic activity as well as disturbed upstream solar wind conditions [*Carpenter et al.*, 1992; *Horwitz et al.*, 1990; *Moldwin et al.*, 2003; *Spasojević et al.*, 2003; *Goldstein et al.*, 2004; *Moldwin et al.*, 2004]. Although the remote sensing instruments of the IMAGE spacecraft are providing unprecedented global views of the plasmasphere and plasma

[1]Universities Space Research Association, Columbia, Maryland, USA.
[2]Heliospheric Physics Branch, NASA Goddard Space Flight Center, Greenbelt, Maryland, USA.

0148-0227/06/2005JA011084

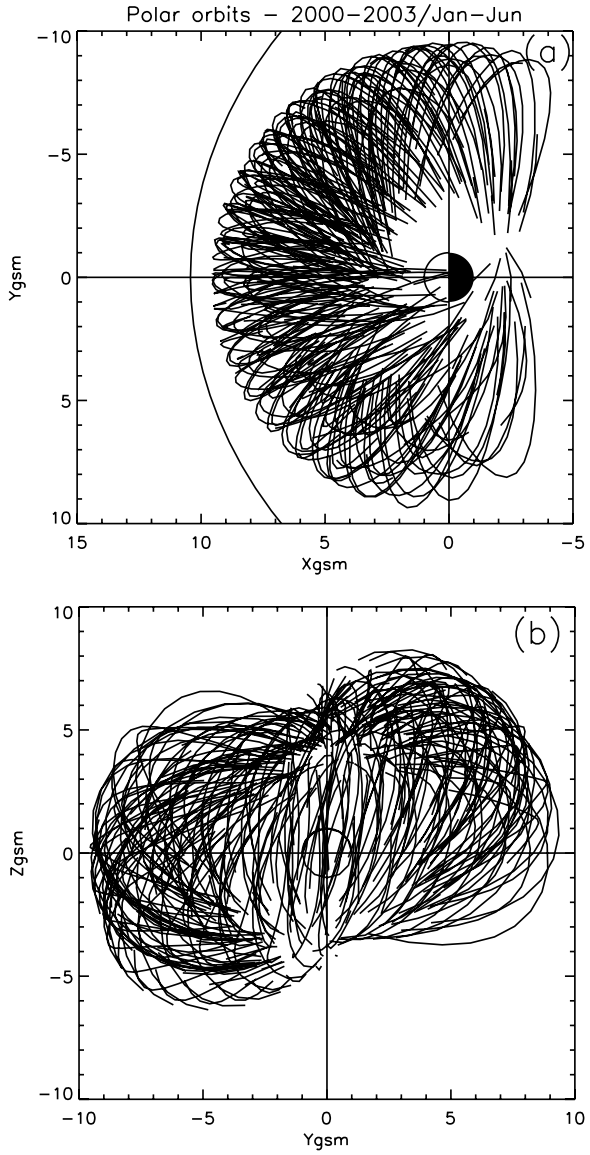

Figure 1. Traces of apogee half orbits (orbits with geocentric distances $r > 5\ R_E$) of Polar spacecraft between 1 January and 30 June of each year from 2000 to 2003 when the thermal ions were surveyed. To reveal more clearly the density of the orbital distributions, only 1 day per every 5 days of orbits is shown, plotted in (a) the *X-Y* GSM plane and (b) the *Y-Z* GSM plane. The model magnetopause of *Shue et al.* [1997] for the solar wind dynamic pressure of 1.8 nano Pascals (nPa), and zero interplanetary magnetic field (IMF) is shown.

plumes, because of the orbit and the instrumentation, the measurements are limited to the inner region and exclude most parts of the outer magnetosphere. Measurements from the Thermal Ion Dynamics Experiment on the Polar spacecraft, with its extended orbits beyond geosynchronous distances, can provide important information about the plasma plumes in the outer region. Although Polar cannot produce large-scale snapshots, since its launch in 1996, the spacecraft has provided numerous outer region samples to enable valid statistical studies.

[4] Our latest discovery of flow bursts of the cold ionospheric ions in the outer magnetosphere by *Chen and Moore* [2004] was limited to the region just inside the magnetopause. To expand our study to include a larger database of the similar events with more pertinent spatial coverage, we have surveyed 3.5 years of Polar Thermal Ion Dynamics Experiment (TIDE) data [*Moore et al.*, 1995] between 2000 and 2003 when the apogee paths were in the dayside outer magnetosphere between 0600–1800 local time (LT) and ±60° latitudes. Although Polar was in a high-inclination orbit where the orbital plane lying at steep angles to the equatorial plane, the apogees of its highly elliptical orbits swung 35° above and below the equatorial plane over the 4-year period. This inclination enabled us to collect measurements in the equatorial plane at locations inside the apogees. Our new data set covers the dayside magnetosphere between the apogees (~9 R_E) and distances just inside the geosynchronous orbit (~5 R_E). Although somewhat deficient in locations at the average magnetopause position (~10 R_E), the data set still contains a significant number of orbits near the magnetopause, as the highly variable solar wind pressure often pushed the magnetopause inside the apogees. With a data set that covers well the space between the magnetopause and the geosynchronous orbit, we are able to better understand the connection between the cold ionospheric ions found at the magnetopause and the plasmaspheric plumes/extensions at distances beyond the geosynchronous orbit. In this paper, we will carry out the statistical analysis on the spatial occurrence of thermal ions, magnetospheric convection patterns and their relationship to the orientation of the interplanetary magnetic field (IMF).

2. Analysis

[5] We have surveyed 3.5 years of Polar TIDE data for thermal ions when the spacecraft was in the dayside outer magnetosphere. Between 1 January and 30 June of each year from 2000 to 2003 the apogee halves of the Polar orbits ($r > 5\ R_E$) covered a wide range of local times between 0600 and 1800 hours and magnetic latitudes of ±60°. Figure 1 shows the orbital projections in the *X-Y* and *Y-Z* geocentric solar magnetospheric (GSM) planes for the period collected. Figure 2 shows the contours of the numbers of equatorial crossings within ±37.5° above or below the *X-Y* GSM plane in 1 R_E by 1-hour local time bins. The number of crossings in each bin represents the summation of the numbers of crossings over five 15° latitudinal bins (one at the equator ±7.5°, two above and two below). Crossings were only counted once per orbit when the spacecraft was present in each bin. The summation over the latitudinal bins increases the chances of detecting thermal ions that might be found above or below the GSM equator, e.g., in the dipole equator [*Takahashi et al.*, 2004]. Most importantly, this also minimizes the orbital biases (see the further discussion below). Using data displays like that of Figure 2 of *Chen and Moore* [2004], we searched for intervals that had the following characteristics: (1) energy spread relatively narrow (~1 eV), (2) peak energy well above the spacecraft potential (a few eV or a few tens of kilometers per second) and below the instrument upper energy threshold (~400 eV or ~300 km s^{-1}), and (3) flow direction perpendicular to the background magnetic field. An important point here is that in the

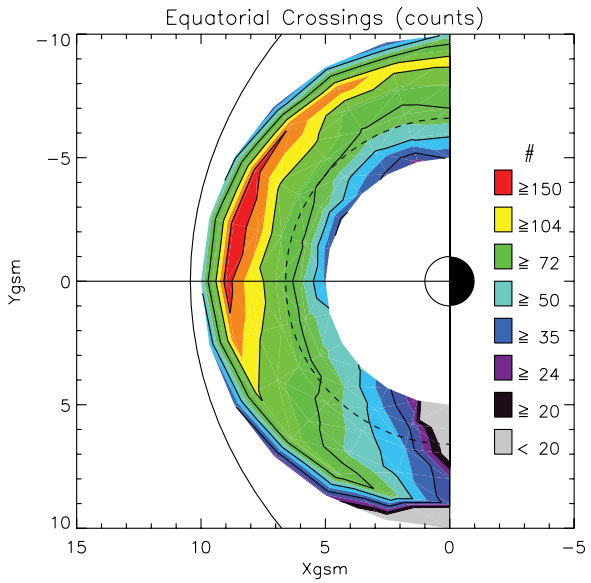

Figure 2. Distribution of the number of equatorial crossings (sum of five 15° latitude bins ±37.5° from $Z_{GSM} = 0$) in 1 R_E × 1-hour magnetic local time (MLT) bins over the period surveyed (Figure 1). The dashed curve is the geosynchronous distance of 6.6 R_E. The contour levels are counts in logarithmic scale. The model magnetopause of *Shue et al.* [1997] for the solar wind dynamic pressure of 1.8 nPa and zero IMF is shown.

summary plots the plasma must have a motion of several kilometers per second relative to the spacecraft to be visible above the spacecraft potential threshold. The effect of the spacecraft potential was corrected in the moment calculation. The spacecraft velocities were negligible (<5 km s^{-1}) compared with the velocity shifts due to the spacecraft potential at distances beyond 5 R_E. We logged the start and stop times when these ions were present continuously or intermittently. The durations of the intervals could be as short as 20 min and as long as 9 hours. We have collected a total of 398 intervals or 887 hours with the presence of thermal ions among more than 12,000 hours of apogee paths surveyed.

[6] We incorporated solar wind data from the ACE spacecraft at the L1 point for the thermal ion collection and introduced time lags based on the simple convection model, i.e., X/V_x. Figure 3 shows the histograms of the solar wind dynamic pressure and the IMF clock and cone angles. The average solar wind dynamic pressure is ∼1.8 nano Pascals (nPa) (black line). The IMF clock angle (red line), angle to the Z axis in the Y-Z GSM plane, has peaks at −110° and 90°. There are slightly more data points for the southward IMF. The IMF cone angle (blue dashed line), angle to the X axis in the X-Y GSM plane, has peaks at −50° and 145°. The majority of the data points have the IMF pointing either away or toward the Sun at an angle of ∼50° from the Sun-Earth line. Our collection of thermal ion events represents a data set that has a typical solar wind dynamic pressure, IMF cone angle and clock angle variations with slightly more data points for the southward IMF.

[7] Figures 4a and 4b show the orbital traces of the 398 thermal ion intervals in GSM coordinates. Significantly more intervals occur at the duskside than at the dawnside. By comparing Figure 4 with Figure 1 and Figure 2 we find there were a good number of equatorial crossings in both the dawnsides and dusksides of the magnetosphere. This assures us in the efforts to minimize the possible orbital biases: the spring seasonal bias (1 January to 30 June) toward $+Z_{GSM}$ at dusk (upper right quadrant of Figure 1b) and $-Z_{GSM}$ at dawn (lower left quadrant) and the epoch bias toward $+Z_{GSM}$ (more apogees above the equatorial plane between 2000 and 2003). Despite a dawnside bias in the orbital coverage, the thermal ions are more likely to be found at the duskside. The dawn-dusk asymmetry in our thermal ion collection is statistically significant. To study the effect of solar wind dynamic pressure on the occurrence, the occurrences were normalized to the same magnetopause-Earth distance at fixed local times according to the solar wind dynamic pressure. Using the magnetopause model of *Shue et al.* [1997], for the average solar wind dynamic pressure of 1.8 nPa (Figure 3) we normalize the local occurrences against the whole thermal ion collection. Figure 4c reveals a radial spreading of the orbits caused by the normalization, but the similar asymmetrical pattern persists.

[8] Figure 4d shows the occurrence rate of thermal ions relative to the whole data set (compare with Figure 2). The contour levels are percentages in a logarithmic scale. The method of counting the orbital presence of thermal ions is the same as described earlier in the paper. Given significantly more orbits at the dawnside (Figure 2), the chances of observing thermal ions were significantly higher at the duskside. The occurrence rate of thermal ions at most locations beyond the geosynchronous orbit (dashed curve in Figure 4d) at the duskside was >10%, compared with ∼0% at the dawnside. The occurrence rate near the duskside magnetopause, particularly at 1300–1600 LT, was >50%, compared with only <30% in a relatively narrow local time sector at the dawnside. The occurrence rate at ∼0900 LT

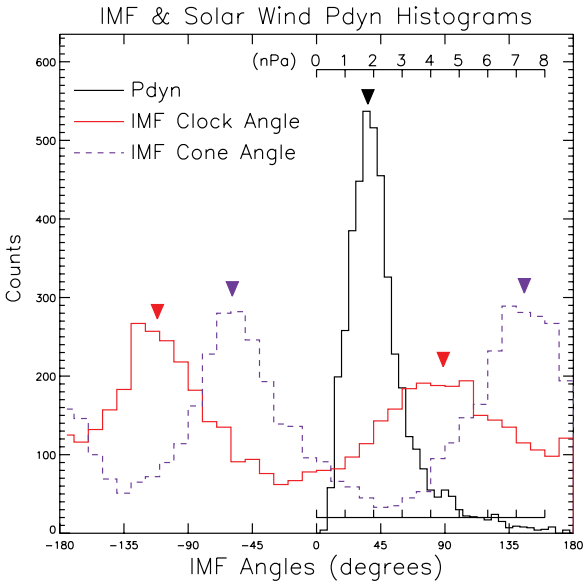

Figure 3. Histograms of solar wind dynamic pressure (black), IMF clock angle (blue dashes), and IMF cone angle (red) in GSM coordinates for thermal ion events.

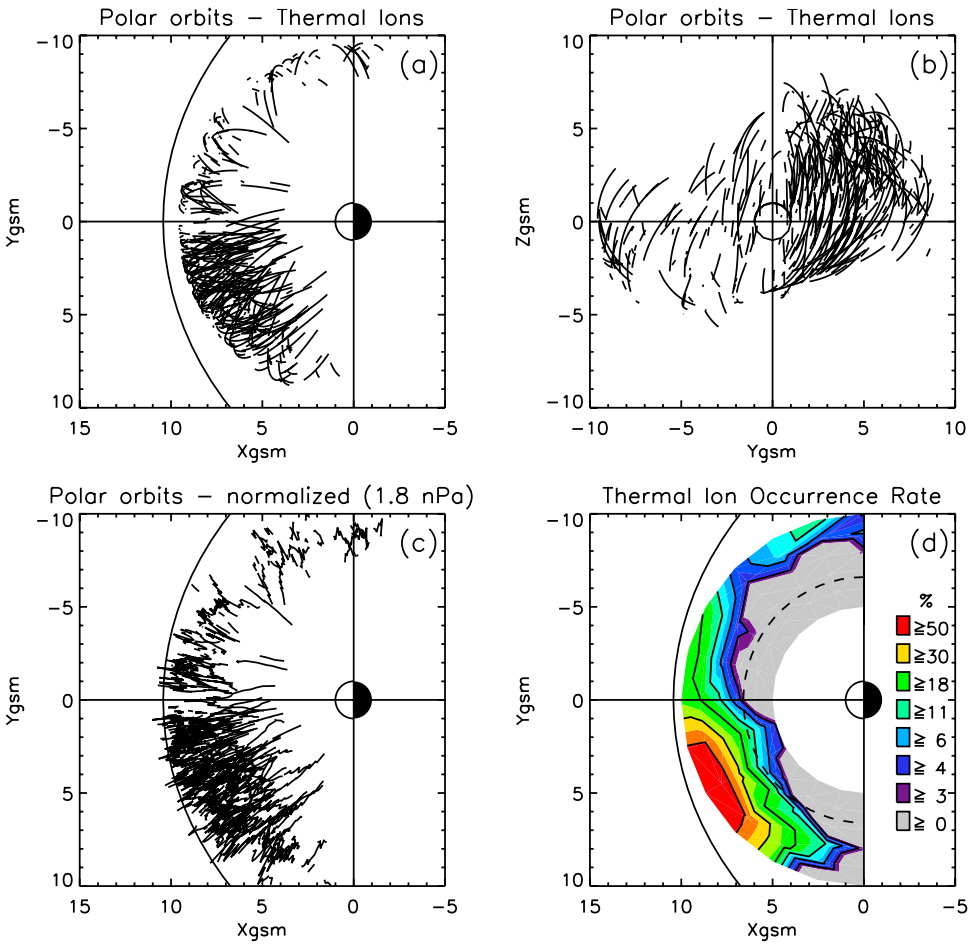

Figure 4. Orbital traces during the intervals when thermal ions were observed, plotted (a) in the *X-Y* GSM plane, (b) in the *Y-Z* GSM plane, and (c) in the *X-Y* GSM plane after the radial distances were normalized by the effect of solar wind dynamic pressure [*Shue et al.*, 1997] at 1.8 nPa and zero IMF. (d) Contours of the occurrence rate of thermal ion events relative to the whole data set surveyed (Figure 2). The dashed curve is the geosynchronous distance of 6.6 R_E. The contour levels are percentages in logarithmic scale. The model magnetopause of *Shue et al.* [1997] is shown.

was extremely low (<5%). A higher thermal ion occurrence rate indicates a higher probability to observe disturbed, either convecting or oscillating, cold thermal ions. Considering the similarities in the spatial distribution and plasma characteristics, the regions of high thermal ion occurrence at the duskside are most likely related to the extension of plasmaspheric drainage plumes at the geosynchronous orbit observed by the IMAGE spacecraft and geosynchronous orbiters [*Sandel et al.*, 2003; *Moldwin et al.*, 2003; *Goldstein et al.*, 2004]. The higher thermal ion occurrences at distances closer to the magnetopause most likely indicate that a more dynamic process is likely to occur at the magnetopause boundary than at the geosynchronous orbit.

[9] The thermal ion event collection is further divided into six categories in terms of IMF clock angle: (1) strongly northward IMF, (2) strongly southward IMF, (3–4) horizontal IMF with the combinations of $\pm B_y$, and (5–6) $\pm B_z$. In each category, the occurrence rate is calculated for each LT radius bin similarly to those shown in Figure 4d. Figure 5 shows the occurrence rates of the thermal ion events for strongly northward IMF or $|\theta_{clock}| \leq 45°$ (Figure 5a) and strongly southward IMF or $|\theta_{clock}| \geq 135°$ (Figure 5b). For strongly northward IMF (Figure 5a) the peak occurrence rate occurs close to the magnetopause at 1300 magnetic local time (MLT). For southward IMF (Figure 5b) the peak occurrence rate occurs near 1400–1500 LT and extends over wider radial distances. The peak occurrence rate for strongly southward IMF (~15%) is about 50% larger than that for strongly northward IMF (~10%). The higher occurrence rate and wider radial spreading for the strongly southward IMF case is consistent with reconnection occurring at the magnetopause near that local time associated with local boundary perturbations [*Le et al.*, 2004]. The similar patterns of occurrences due to the polarity of IMF B_z occur when the IMF is mostly horizontal oriented but only patched with additional details. Figure 6 shows the occurrences for the horizontal IMF for the combinations of $\pm B_y$ and $\pm B_z$: IMF $B_z > 0$ and IMF $B_y < 0$ or $-90° \leq \theta_{clock} < -45°$ (Figure 6a), IMF $B_z > 0$ and IMF $B_y > 0$ or $45° < \theta_{clock} \leq 90°$ (Figure 6b), IMF $B_z < 0$ and IMF $B_y < 0$ or $-135° < \theta_{clock} < -90°$ (Figure 6c), and IMF $B_z < 0$ and IMF $B_y > 0$ or $90° < \theta_{clock} < 135°$ (Figure 6d). When the IMF B_z changes sign (by comparing Figures 6a to 6c and 6b to 6d), there are higher occurrences found of local time shifts and radial

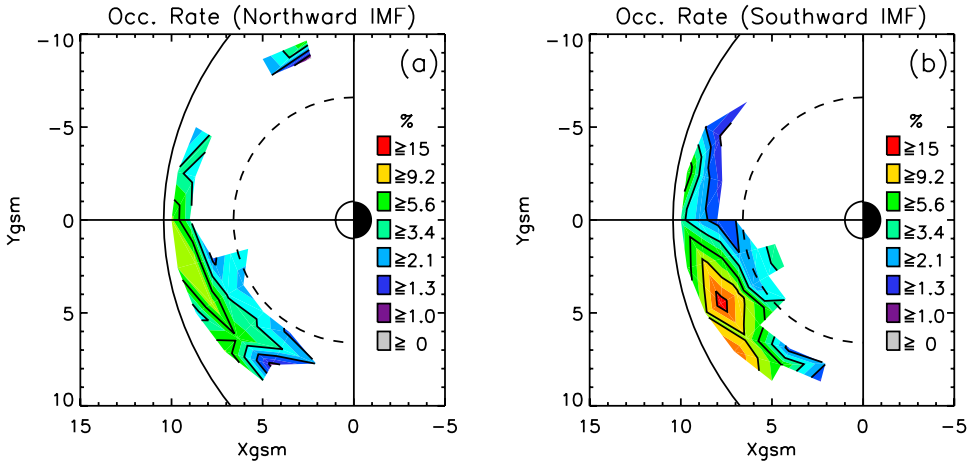

Figure 5. Contours of the occurrence rates of the thermal ion events, same as Figure 4d but for (a) northward IMF, $|\theta_{clock}| \leq 45°$ and (b) southward IMF, $|\theta_{clock}| \geq 135°$.

spreading than for strongly northward to southward turning of the IMF. Conversely, with the same sign of IMF B_z (by comparing Figures 6a to 6b and 6c to 6d) the changes in the occurrences due to the sign of IMF B_y are visible though small. They indicate single peak distributions when IMF B_y is negative (Figures 6a and 6c) but multiple peaks separated in local times when IMF B_y is positive (Figures 6b and 6d). They also indicate slight shifts in the major distributions to

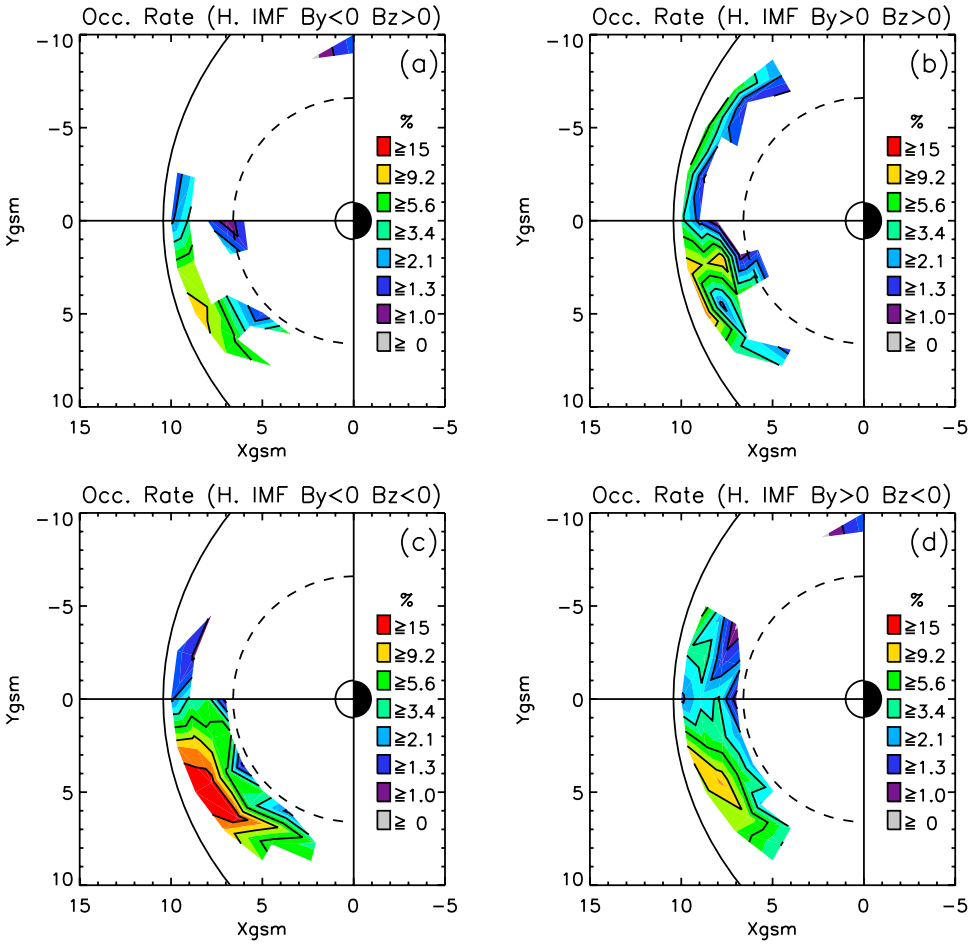

Figure 6. Contours of the occurrence rates of the thermal ion events, same as Figure 4d but for the horizontal IMF conditions (a) IMF $B_y < 0$ and IMF $B_z > 0$, $-90° \leq \theta_{clock} < -45°$, (b) IMF $B_y > 0$ and IMF $B_z > 0$, $45° < \theta_{clock} \leq 90°$, (c) IMF $B_y < 0$ and IMF $B_z < 0$, $-135° < \theta_{clock} < -90°$, and (d) IMF $B_y > 0$ and IMF $B_z < 0$, $90° < \theta_{clock} < 135°$.

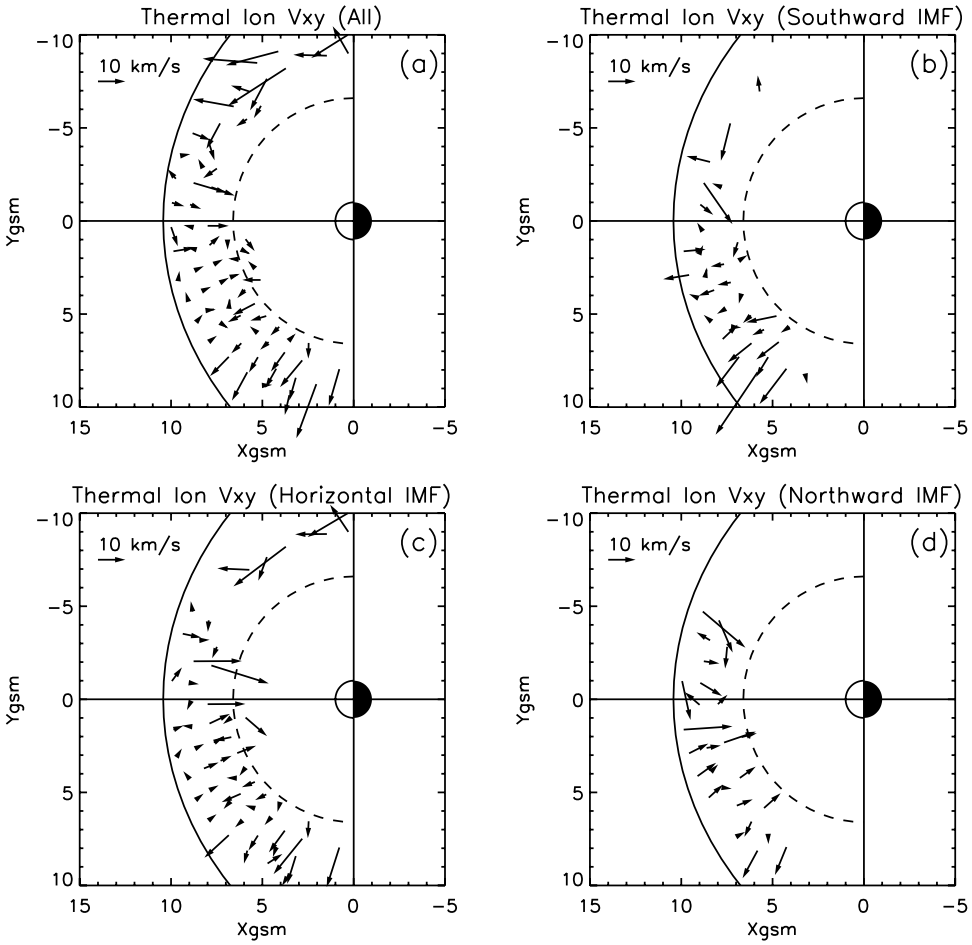

Figure 7. Dayside magnetospheric convection pattern in the *X-Y* GSM plane represented by the averaged thermal ion flow vectors during intervals of various IMF orientations. The arrow in each local time (LT) radius bin represents the averaged thermal ion flow vector occurring with ±45° latitudes while each occurrence is the 10-min average of 6-s measurements. There are at least 10 occurrences in each bin for averaging. Otherwise it is treated as a data gap. The empty bins shown in Figure 7 are data gaps but not stagnant. (a) All cases. (b) Southward IMF, $|\theta_{clock}| \geq 135°$. (c) Horizontal IMF, $45° < |\theta_{clock}| < 135°$. (d) Northward IMF, $|\theta_{clock}| \leq 45°$.

the dawnside when IMF B_y changes from negative to positive (from Figure 6a to 6b or from Figure 6c to 6d). The direction of the shifts is consistent with the direction of force exerted on inter-reconnected IMF magnetic flux tubes. The additional peaks at the dawnside or, equivalently, the splitting and spreading of the major peak at 1400–1500 LT, when IMF B_y is positive (Figures 6b and 6d), may indicate a higher thermal ion or plasma convection strength is likely to occur where the reconnected flux tubes traverse the magnetopause.

[10] Generally, when the center of the velocity distributions falls within the sensitivity range of the instrument, the measured dense thermal ions represent the bulk of the plasma population's mass density. Consequently, the perpendicular component of the thermal ion flow vector to the magnetic field becomes a good indicator of the motion of the magnetic field line, since the plasma frozen-in condition applies (see discussion in Appendix A). Such motions are driven by force balance between the plasma pressure gradients and Maxwell stresses and ionospheric drag. The composition of the average flow vectors of local time radial bins at various solar wind conditions help us to depict the convection patterns of the magnetosphere under these conditions. We calculate the equatorial component of the thermal ion flow vector in the equatorial plane for different IMF orientations. Figure 7 shows the flow patterns in the *X-Y* GSM plane at various IMF orientations: all cases (Figure 7a), southward IMF, $|\theta_{clock}| \geq 135°$ (Figure 7b), horizontal IMF, $45° < |\theta_{clock}| < 135°$ (Figure 7c), and northward IMF, $|\theta_{clock}| \leq 45°$ (Figure 7d). The arrow in each LT radius bin represents the average projection of flow vector in the *X-Y* GSM plane that occurred within ±45° latitudes, while each occurrence is a 10-min average of 6-s TIDE measurements. We only show bins that have at least 10 occurrences. Otherwise they are treated as data gaps (nothing shown). Because of instrument limitations [*Chen and Moore*, 2004], the polar angle distribution is collapsed into the spin plane projection. As a result, we only calculated the two spin plane components of the flow vectors. The sign of the two spin plane components (close to the radial and the Z_{GSM} components in the equatorial plane) should remain unaffected. The magnitude of the radial

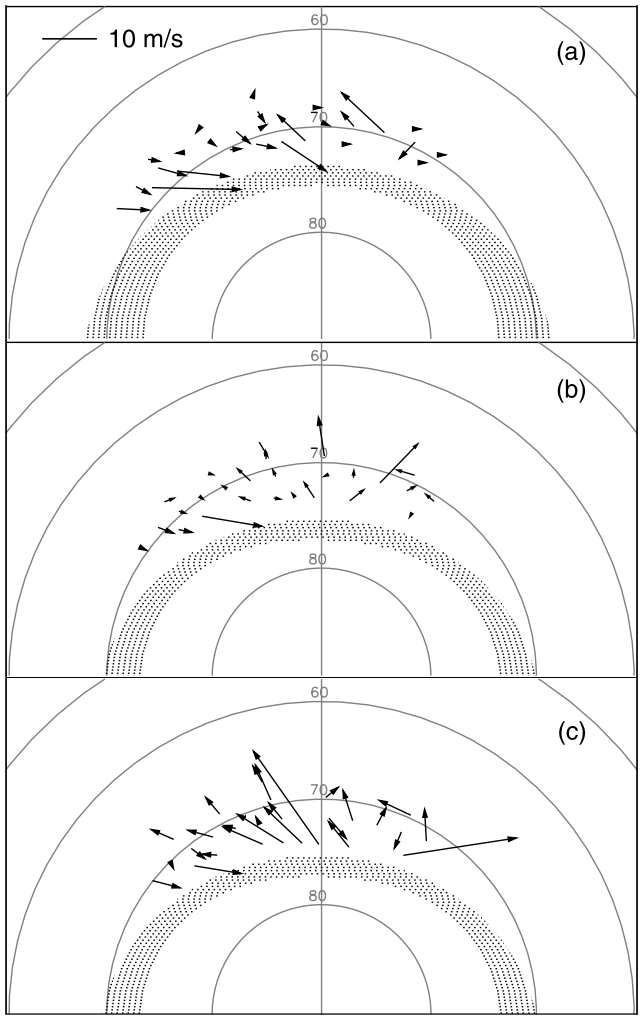

Figure 8. Dayside equatorial magnetospheric convection patterns mapped to the surface of the Earth for (a) southward IMF (compare with Figure 7b), (b) horizontal IMF (compare with Figure 7c), and (c) northward IMF (compare with Figure 7d). The Tsyganenko 2001 magnetic field model [*Tsyganenko*, 2002] is used and model auroral ovals (dotted areas) of *Holzworth and Meng* [1975] are overlaid. (Refer to the text for the parameters used in these models.)

component of flow vectors is somewhat overestimated if the out-of-spin-plane component is significant. However, according to about 6 months of data when the spin plane was in the equatorial plane [*Chen and Moore*, 2004], the azimuthal component of the flow vectors in the outer magnetosphere is generally less than the radial component, if not much smaller. The spin-plane collapsing effect on the estimate of the flow speed is not overwhelmingly significant in the cases studies here. Figure 7a shows that for all the cases the flow velocities are mostly less than 10 km s^{-1} in the subsolar local time sector and largely enhanced to a few tens of kilometers per second at the flanks. When the IMF is southward (Figure 7b), the flow velocities in the afternoon sector are on average sunward (averaged V_x = 1.2 km s^{-1}, V_y = 0.2 km s^{-1}) and much enhanced toward the dusk flank (averaged V_x = 7.3 km s^{-1}, V_y = 7.5 km s^{-1}). There is a clear boundary near 1500 LT that separates the slow from the fast sunward convection. Conversely, when the IMF is northward (Figure 7d), the flow velocity vectors in the afternoon local time sector are mainly earthward (averaged $V_x = -5.6$ km s^{-1}, $V_y = -2.7$ km s^{-1}) and largely reduced near the dusk flank (averaged V_x = 0.6 km s^{-1}, V_y = 3.7 km s^{-1}). A stagnation local time boundary can be identified near 1600 LT. The variation of the convection pattern due to the changing in the orientation of the IMF is consistent with the equatorward and poleward reconnection scenarios that drive the dayside convection, superposed on background convection (driven by a not-well-understood viscous interaction), combined with corotation of the Earth's magnetic field with the ionospheric plasma.

[11] To understand how the magnetospheric convection links to the ionospheric convection, we map the flow vectors in the equatorial plane to the surface of the Earth. We use the Tsyganenko 2001 magnetic field model [*Tsyganenko*, 2002] to trace the field lines connecting the two. Figure 8 shows the convection patterns on the surface of the Earth for, from top to bottom, southward, horizontal, and northward IMF. To each case respectively, we apply parameter sets consisting of solar wind dynamic pressure, *Dst* index, IMF B_y, IMF B_z, and current indices: {1.8 nPa, −30 nT, 0, −5 nT, 10, 10} (Figure 8a), {1.8 nPa, −10 nT, 0, 0, 3, 6} (Figure 8b), and {1.8 nPa, 0, 0, 5 nT, 2, 3} (Figure 8c). For all the three cases, we set the model field at 2200 UT on the 80th day of 2002 when the dipole was close to the spring equinox. We also overlay model auroral ovals (dot-filled areas) [*Holzworth and Meng*, 1975] for high (IQL = 4), medium (IQL = 3), and low (IQL = 2) geomagnetic activities. When the IMF is southward (Figure 8a), convection in the afternoonside is mainly pointing toward the noon-midnight plane with poleward components. This is consistent with reconnection occurring equatorward of the cusps over a wide range of local times in the dayside magnetopause and bringing magnetic fluxes over high latitudes to the nightside. When the IMF is horizontal (Figure 8b), the convection speeds subside and the directions become less organized. When the IMF is northward (Figure 8c), the convection in the afternoonside is mainly equatorward. This is consistent with reconnection at high latitudes poleward of the cusps, bringing magnetic fluxes to the dayside. The directions of convection are reversed when the IMF changes from southward to northward.

3. Discussion

[12] While the dawn-dusk asymmetry is prominent, the lower occurrence rates at closer geocentric distances, particularly within geosynchronous orbit, are biased by the lack of equatorial sampling. When we look at the occurrence of cold thermal ions in the L shell against radial distances, we find that that most of the data points within $5 < r < 7\ R_E$ have their L shell values >7. In other words, these data points are mostly coming from higher latitudes. The implication is that, at higher latitudes, the chance to observe the thermal ions is smaller than in the equatorial plane. Another possible explanation is that the lower occurrence rates at closer distances might be due to small thermal ion convection speeds that were not detectable by the instrument.

[13] *Chappell* [1972] studied the thermal ions (~1 eV) in the magnetosphere using data from the ion mass spectrometer on the OGO 5 spacecraft. He discovered that the possibility to observe the thermal ion density enhancements in the plasma trough between the plasmapause and the magnetopause, described as detachments from the plasmasphere in the paper, was greater at the duskside than at the dawnside. He showed that, out of a total of 202 plasma trough crossings distributed over a wide range of local times including dayside and nightside, there were 49 instances of detached plasmas that have densities exceeding 10 ions cm^{-3}, 2 orders of magnitude larger than the instrument noise level. Of these occurrences, 41 or 84% were found in the dayside sector 0600–1920 LT. Of these occurrences, 31 or 76% were located in the afternoon-dusk sector 1240–1920 LT. Although based upon a smaller database that did not extend to the magnetopause region, the dawn-dusk asymmetry found in this paper is consistent with what we have found.

[14] The pioneering works of *Kavanagh et al.* [1968], *Grebowsky* [1970], and *Chen and Wolf* [1972] revealed convection patterns similar to those found in our study. To interpret the plasma plumes that OGO 5 observed, these earlier studies mathematically formulated the process of the generation and evolution of plasma plumes (known then as plasma tails) by constructing an electric field model through the superposition of a corotation electric field and a dawn-dusk electric field. The corotation electric field is induced by the relative motion of the Earth's ionosphere rotating with the Earth and is mapped outward by equipotential magnetic field lines. The dawn-dusk electric field was set to vary with *Kp*. Qualitatively, their interpretation is generally in good agreement with the observations. Although, the plasma plumes evolution timescale they found (6 days) was longer than what IMAGE has observed (few hours), their models have provided a good perspective on the drivers for magnetospheric convection and have provided interpretations for how the thermal ions might originate and why they are more likely to be observed at the duskside.

[15] By analyzing the SuperDARN radar measurements, *Ruohoniemi and Baker* [1998] discovered a rapid reconfiguration of global convection patterns in the polar ionosphere in response to the sudden changes in the polarity of IMF B_z (Figure 8). They presented a few examples of the reconfiguration of global convection patterns in <6 min timescales as the IMF suddenly changed from northward to southward or vice versa. They showed that when the IMF was southward the ionospheric convection-borne two-cell pattern with dominantly tailward convection, sunward if mapped to the equatorial plane, in the noon-midnight cross–polar cap channel. Ruohoniemi and Baker explained that the convection pattern was a result of reconnection at the subsolar magnetopause, which brings magnetic flux over the polar cap to the nightside. When the IMF was northward, the two-cell pattern became highly distorted and then cascaded to a few smaller cells. The tailward convection in the cross–polar cap channel near the noon-midnight meridian plane disappeared and became convecting sunward, tailward if mapped to the equatorial plane, in a smaller region (~10° latitude) near the cusp. Ruohoniemi and Baker explained that the pattern was a result of reconnection at the high-latitude magnetopause poleward of the cusps. Their finding of the convection pattern changes near the cusp in response to the polarity of IMF B_z is qualitatively consistent with what we have found.

[16] Using the electric field measurements on the Combined Release and Radiation Effects Satellite (CRRES) spacecraft, *Wygant et al.* [1998] studied the role of large spatial-scale electric fields in creating the ring current. In the study, they looked at a case when the main phase of a major geomagnetic storm ($Dst \sim -300$ nT) and the dawn-to-dusk electric field reached 6 mV m^{-1}, a factor of 60 or more times greater than the average quiet time value, at the duskside between $L = 2$ and $L = 4$. This was an extreme case, but demonstrates that the sunward convection at the duskside can be highly enhanced and its earthward boundary, the separatrix of close and open drift paths, can reach a distance as close as $L = 2$, deep into the region where the corotation electric field dominates. The strong dawn-to-dusk electric field reflects drainage of cold plasmaspheric ions into the outer magnetosphere and into the solar wind via reconnection at the magnetopause. The result is similar to the paths of the plasma plumes found in our study.

[17] *Matsui et al.* [2003, 2004] derived the electric potential patterns in the inner magnetosphere ($4 < L < 10$) using 2 years (about twice the full coverage of all local times) of electric field measurements from electron drift instruments (EDI) on the Cluster spacecraft. Assuming equal potential on the same magnetic field lines, they derived the electric field, $\mathbf{E} \times \mathbf{B}$ drift vectors, and the electric potential in the equatorial plane with either in-equator or out-of-equator electric field measurements. The electric potential obtained in their study indicates a strong dependence on the polarity of IMF B_z. The sunward convection in the outer region near $L = 10$ was enhanced at all local times including the afternoon sector for negative IMF B_z over positive IMF B_z (Figure 5b of *Matsui et al.* [2003]), which is similar to what we have found. However, there was no earthward convection in the afternoon sector near the magnetopause ($L = 10$) in Matsui et al.'s categorization of positive IMF B_z [*Matsui et al.*, 2003, Figure 5d]. Although the cross calibration between, and assumptions imposed, the measured-or-derived EDI electric field and the velocity moments of TIDE both need to be verified, it is possible that this relatively minor inconsistency is caused by the way they organized the data. Matsui et al. classified their data set into only two categories of IMF clock angle (IMF $B_z > 0$ and IMF $B_z < 0$), instead of three. As a result, the effects from horizontal IMF could have been significant and the flow reversals might have been smoothed out.

[18] Many studies have reached the same conclusion: that solar wind drives the magnetospheric convection. It is, however, not well understood precisely what processes as well as time and spatial scales are involved. Moreover, it is also not clear to what degrees these processes are important, e.g., how do they contribute to the magnetospheric system's total mass and energy. According to our current and previously related studies [e.g., *Chen and Moore*, 2004], as well as studies from the IMAGE spacecraft [e.g., *Sandel et al.*, 2003], we now know that the cold thermal ions in the inner magnetosphere can reach out to a broad local time sector from the subsolar to the duskside near the magnetopause in a timescale of a few hours, as suggested by *Freeman et al.* [1977]. The cold thermal ion particle fluxes are comparable with the incoming fluxes from the magneto-

sheath; therefore the cold thermal ions are dynamically important to the boundary processes, such as reconnection and viscous interaction, at the magnetopause and contribute significantly to the magnetospheric system's total mass.

[19] The most obvious significance of cold plasma presence in the region of dayside reconnection lies in its substantial impact on the local Alfvén speed [*Chen and Moore*, 2004]. The density of plasmaspheric plasma in this region ranges from <0.1 cm^{-3} to nearly 100 cm^{-3}, in response to the intensity and depth of magnetospheric convection. During active times, the fraction of O^+ in the plasma is likely to be enhanced by auroral processes, further enhancing its mass density. Recently there has been considerable interest in the apparent saturation of the transpolar potential during large geospace storms [*Siscoe et al.*, 2004]. Mass loading by ionospheric plasma has been suggested as one mechanism to effect this saturation [*Winglee et al.*, 2002], on the basis of the first global simulations to include ionospheric plasmas as a dynamical element. We suggest here that the enhancement of dayside plasma densities by ionospheric material convected from the plasmasphere, is likely to limit the possible rate of reconnection, with a moderating influence on global magnetospheric convection, as measured by the transpolar potential. Apart from this effect on dayside reconnection, these ionospheric plasmas are also bound to be convected through the polar caps and lobes into the magnetotail, as suggested by a number of recent works, including, quite recently, *Foster et al.* [2004].

4. Conclusion

[20] After having surveyed 3.5 years of thermal ion measurement from the TIDE instrument on the Polar spacecraft, we have found a dawn-dusk asymmetry of the occurrence of thermal ions and magnetospheric convection patterns that are a function of IMF clock angles in the dayside outer magnetosphere. Significantly more thermal ion events occurred at the duskside than at the dawnside, consistent with the extension of plasmaspheric drainage plumes away from the dusk region near geosynchronous orbit toward the magnetopause. Particularly at the 1300–1600 LT sector, the occurrence rate increases from ~20% at geosynchronous orbit to 50% or higher near the magnetopause, compared with the highest occurrences of ~0% to ~30% in the prenoon sector at the dawnside. In the ~0900 LT sector near the magnetopause, the occurrence rate is extremely low (<5%). A higher thermal ion occurrence rate indicates a higher chance to observe dynamically disturbed cold ions, whether convecting or in periodic motion. Because of the spatial distribution and the plasma characteristics, we interpret these thermal ion events as reflecting the extension of the plasmaspheric drainage plumes carrying cold plasmaspheric ions sunward. The higher thermal ion occurrence rate at the duskside magnetopause is significant in the local plasma conditions for reconnection [*Chen and Moore*, 2004; *Le et al.*, 2004], which is related to enhanced strength of convection at the duskside [*Carpenter et al.*, 1992; *Foster and Vo*, 2002; *Goldstein et al.*, 2003b]. As convection drains more cold ions from the plasmasphere, convecting sunward and supplying cold ions at the magnetopause boundary, the rate of reconnection at the magnetopause will be affected by the alteration of the local Alfvén speed. Assuming reconnection at a relatively constant fraction of that local limit, the rate of reconnection would be moderated by the presence of a substantial mass density enhancement from the cold plasmaspheric material [*Hesse and Birn*, 2004]. This process could substantially influence the dynamo process in the global magnetospheric convection, with a similar dawn-dusk asymmetry. The variation of the observed convection pattern owing to the orientation of the IMF is consistent with equatorward and poleward reconnection scenarios that drive the dayside convection, superposed on background convection (driven by a viscous interaction), combined with corotation of the Earth's magnetic field with the ionosphere.

Appendix A. Validity of Frozen-in Condition in the Dayside Outer Magnetosphere

[21] The generalized Ohm's law with the following assumptions: (1) singly charged ions, (2) all ions have the same mass m_i, (3) ion mass is much larger than electron's $m_i >> m_e$, and (4) charge neutrality $\rho_c \mathbf{v} << \mathbf{j}$ is

$$\mathbf{E} = -\mathbf{v}\times\mathbf{B} + \frac{1}{ne}\mathbf{j}\times\mathbf{B} + \eta\mathbf{j} - \frac{1}{ne}\nabla\cdot\mathbf{p}_e + \frac{m_e}{ne^2}\left[\frac{\partial\mathbf{j}}{\partial t} + \nabla(\mathbf{j}\mathbf{v} + \mathbf{v}\mathbf{j})\right], \tag{A1}$$

where $\rho_c = ne$ is the charge density, n is the number density, η is resistivity, and $\mathbf{p}_e$ is the electron pressure tensor [*Siscoe*, 1983]. Since the thermal ions in the outer magnetosphere have temperatures of the order of 1 eV, the TIDE instrument detected fairly well the whole Gaussian distributions if the peak energies are fall inside the instrument energy range of a few to ~400 eV. With the minimum contribution of hot plasma (keV and above) that are susceptible to local wave-particle interactions and plasma instabilities, the plasma velocity moment V_{TIDE} calculated from TIDE has less uncertainty than using the one with hot plasma components included, that is, V_{TIDE} instead of $V_{\mathrm{TIDE+hot}}$ is closer to the value of $\mathbf{v}$ in (A1). In the dayside outer magnetosphere away from the plasmasphere, $\mathbf{j}$, its spatial and temporal derivatives and $\nabla\,\mathbf{p}_e$ are weak compared with the equivalent quiet time convection electric field of ~1 mV m^{-1}. According to *Jorgensen et al.* [2004], $|\mathbf{j}| < 5$ nA m^{-2} and assuming $n \approx 10$ cm^{-3}, the second term in (A1) without the cross-product with $\mathbf{B}$ becomes

$$\frac{1}{ne}|\mathbf{j}| \approx \frac{5\times10^{-9}(\mathrm{Am}^{-2})}{10\times10^{6}(\mathrm{m}^{3})\times1.6\times10^{-19}(\mathrm{C})} \approx 3\ \mathrm{km\ s}^{-1}. \tag{A2}$$

By assuming weak current density and small resistivity η the third term is also neglected. Assuming $\Delta v \approx 10$ km s^{-1}, $\Delta j \approx |\mathbf{j}|$, the characteristic interval of the time derivative $\Delta t \approx 1$ hour and the characteristic length of the spatial gradient $\Delta L \approx 1\ R_E$, the last two terms in (A1) are approximated as

$$\frac{m_e}{ne^2}\frac{\partial\mathbf{j}}{\partial t} \approx \left|\frac{m_e\Delta j}{ne^2\Delta t}\right| \approx \left|\frac{9\times10^{-31}(\mathrm{kg})\times5\times10^{-9}(\mathrm{Am}^{-2})}{10\times10^{6}(\mathrm{m}^{-3})\times[1.6\times10^{-19}]^2(\mathrm{C}^2)\times3600(\mathrm{sec})}\right| \approx 10^{-8}\mathrm{mV\ m}^{-1} \tag{A3}$$

and

$$\frac{m_e}{ne^2}\nabla(\mathbf{jv}+\mathbf{vj}) \approx \left|\frac{m_e\Delta(jv)}{ne^2\Delta L}\right| \approx 10^{-7}\text{mV m}^{-1}. \qquad \text{(A4)}$$

Assuming $\Delta n/n \sim 1$, $T_e \sim 10$ eV, and again $\Delta L \sim 1\ R_E$, the fourth term, pressure gradient for electrons, in (A1) is approximated as

$$\frac{1}{ne}\nabla \quad \mathbf{p}_e \approx \left|\frac{\Delta(nkT_e)}{ne\Delta L}\right| \approx 10^{-3}\text{mV m}^{-1}. \qquad \text{(A5)}$$

Therefore the terms after $-\mathbf{v} \times \mathbf{B}$ in equation (A1) are negligible. This leads to the frozen-in condition $\mathbf{E} = -\mathbf{v} \times \mathbf{B}$.

[22] **Acknowledgments.** This work was supported by the Polar mission under UPN 370-08-43. We thank D. J. McComas at Southwest Research Institute and N.F. Ness at Bartol Research Institute for making ACE solar wind and magnetic field data available through CDAWeb at NSSDC of NASA GSFC.

[23] Arthur Richmond thanks Hiroshi Matsui and another reviewer for their assistance in evaluating this paper.

References

Carpenter, D. L., A. J. Smith, B. L. Giles, C. R. Chappell, and P. M. E. Decreau (1992), A case study of plasma in the dusk sector associated with enhanced magnetospheric convection, *J. Geophys. Res.*, *97*, 1157.

Chappell, C. R. (1972), Recent satellite measurements of the morphology and dynamics of the plasmasphere, *Rev. Geophys.*, *10*, 951.

Chen, A. J., and J. M. Grebowsky (1974), Plasma tail interpretations of pronounced detached plasma regions measured by OGO 5, *J. Geophys. Res.*, *79*, 3851.

Chen, A. J., and R. A. Wolf (1972), Effects on the plasmasphere of a time-varying convection electric field, *Planet. Space Sci.*, *20*, 483.

Chen, S.-H., and T. E. Moore (2004), Dayside flow bursts in the Earth's outer magnetosphere, *J. Geophys. Res.*, *109*, A03215, doi:10.1029/2003JA010007.

Foster, J. C., and H. B. Vo (2002), Average characteristics and activity dependence of the subauroral polarization stream, *J. Geophys. Res.*, *107*(A12), 1475, doi:10.1029/2002JA009409.

Foster, J. C., A. J. Coster, P. J. Erickson, F. J. Rich, and B. R. Sandel (2004), Stormtime observations of the flux of plasmaspheric ions to the dayside cusp/magnetopause, *Geophys. Res. Lett.*, *31*, L08809, doi:10.1029/2004GL020082.

Freeman, J. W., H. K. Hills, T. W. Hill, P. H. Reiff, and D. A. Hardy (1977), Heavy ion circulation in the Earth's magnetosphere, *Geophys. Res. Lett.*, *4*, 195.

Goldstein, J., M. Spasojević, P. H. Reiff, B. R. Sandel, W. T. Forrester, D. L. Gallagher, and B. W. Reinisch (2003a), Identifying the plasmapause in IMAGE EUV data using IMAGE RPI in situ steep density gradients, *J. Geophys. Res.*, *108*(A4), 1147, doi:10.1029/2002JA009475.

Goldstein, J., B. R. Sandel, M. R. Hairston, and P. H. Reiff (2003b), Control of plasmaspheric dynamics by both convection and sub-auroral polarization stream, *Geophys. Res. Lett.*, *30*(24), 2243, doi:10.1029/2003GL018390.

Goldstein, J., B. R. Sandel, M. F. Thomsen, M. Spasojević, and P. H. Reiff (2004), Simultaneous remote sensing and in situ observations of plasmaspheric drainage plumes, *J. Geophys. Res.*, *109*, A03202, doi:10.1029/2003JA010281.

Grebowsky, J. M. (1970), Model study of plasmapause motion, *J. Geophys. Res.*, *75*, 4329.

Hesse, M., and J. Birn (2004), On the cessation of magnetic reconnection, *Ann. Geophys.*, *22*, 603.

Holzworth, R. H., and C.-I. Meng (1975), Mathematical representation of the auroral oval, *Geophys. Res. Lett.*, *2*, 377.

Horwitz, J. L., R. H. Comfort, and C. R. Chappell (1990), A statistical characterization of the plasmasphere density structure and boundary locations, *J. Geophys. Res.*, *95*, 7937.

Jorgensen, A. M., H. E. Spence, W. J. Hughes, and H. J. Singer (2004), A statistical study of the global structure of the ring current, *J. Geophys. Res.*, *109*, A12204, doi:10.1029/2003JA010090.

Kavanagh, L. D., Jr., J. W. Freeman Jr., and A. J. Chen (1968), Plasma flow in the magnetosphere, *J. Geophys. Res.*, *73*, 5511.

Le, G., et al. (2004), Coordinated polar spacecraft, geosynchronous spacecraft, and ground-based observations of magnetopause processes and their coupling to the ionosphere, *Ann. Geophys.*, *22*, 4329.

Matsui, H., J. M. Quinn, R. B. Torbert, V. K. Jordanova, W. Baumjohann, P. A. Puhl-Quinn, and G. Paschmann (2003), Electric field measurements in the inner magnetosphere by Cluster EDI, *J. Geophys. Res.*, *108*(A9), 1352, doi:10.1029/2003JA009913.

Matsui, H., V. K. Jordanova, J. M. Quinn, R. B. Torbert, and G. Paschmann (2004), Derivation of electric potential patterns in the inner magnetosphere from Cluster EDI data: Initial results, *J. Geophys. Res.*, *109*, A10202, doi:10.1029/2003JA010319.

Moldwin, M. B., B. R. Sandel, M. F. Thomsen, and R. C. Elphic (2003), Quantifying global plasmaspheric images with in situ observations, *Space Sci. Rev.*, *109*, 47.

Moldwin, M. B., J. Howard, J. Sanny, J. D. Bocchicchio, H. K. Rassoul, and R. R. Anderson (2004), Plasmaspheric plumes: CRRES observations of enhanced density beyond the plasmapause, *J. Geophys. Res.*, *109*, A05202, doi:10.1029/2003JA010320.

Moore, T. E., et al. (1995), The thermal ion dynamics experiment and plasma source instrument, *Space Sci. Rev.*, *71*, 409.

Ruohoniemi, J. M., and K. B. Baker (1998), Large-scale imaging of high-latitude convection with Super Dual Auroral Radar Network HF radar observations, *J. Geophys. Res.*, *103*, 20,797.

Sandel, B. R., R. A. King, W. T. Forrester, D. L. Gallagher, A. L. Broadfoot, and C. C. Curtis (2001), Initial results from the IMAGE extreme ultraviolet imager, *Geophys. Res. Lett.*, *28*, 1439.

Sandel, B. R., J. Goldstein, D. L. Gallagher, and M. Spasojević (2003), Extreme ultraviolet imager observations of the structure and dynamics of the plasmasphere, *Space Sci. Rev.*, *109*, 25.

Shue, J.-H., J. K. Chao, H. C. Fu, C. T. Russell, P. Song, K. K. Khurana, and H. J. Singer (1997), A new functional form to study the solar wind control of the magnetopause size and shape, *J. Geophys. Res.*, *102*, 9497.

Siscoe, G. L. (1983), Solar system magnetohydrodynamics, in *Solar-Terrestrial Physics*, edited by R. L. Carovillano and J. M. Forbes, pp. 11–100, Springer, New York.

Siscoe, G., J. Raeder, and A. J. Ridley (2004), Transpolar potential saturation models compared, *J. Geophys. Res.*, *109*, A09203, doi:10.1029/2003JA010318.

Spasojević, M., J. Goldstein, D. L. Carpenter, U. S. Inan, B. R. Sandel, M. B. Moldwin, and B. W. Reinisch (2003), Global response of the plasmasphere to geomagnetic disturbance, *J. Geophys. Res.*, *108*(A9), 1340, doi:10.1029/2003JA009987.

Takahashi, K., R. E. Denton, R. R. Anderson, and W. J. Hughes (2004), Frequencies of standing Alfvén wave harmonics and their implication for plasma mass distribution along geomagnetic field lines: Statistical analysis of CRRES data, *J. Geophys. Res.*, *109*, A08202, doi:10.1029/2003JA010345.

Tsyganenko, N. A. (2002), A model of the near magnetosphere with a dawn-dusk asymmetry: 2. Parameterization and fitting to observations, *J. Geophys. Res.*, *107*(A8), 1176, doi:10.1029/2001JA000220.

Winglee, R. M., D. Chua, M. Brittnacher, G. K. Parks, and G. Lu (2002), Global impact of ionospheric outflows on the dynamics of the magnetosphere and cross-polar cap potential, *J. Geophys. Res.*, *107*(A9), 1237, doi:10.1029/2001JA000214.

Wygant, J., D. Rowland, H. J. Singer, M. Temerin, F. Mozer, and M. K. Hudson (1998), Experimental evidence on the role of the large spatial scale electric field in creating the ring current, *J. Geophys. Res.*, *103*, 29,527.

S.-H. Chen, Heliospheric Physics Branch, Code 612.2, NASA Goddard Space Flight Center, Greenbelt, MD 20771, USA. (sheng-hsien.chen@gsfc.nasa.gov)

T. E. Moore, Heliospheric Physics Branch, Code 612.2, NASA Goddard Space Flight Center, Greenbelt, MD 20771, USA.